13.3 COMPARISON BETWEEN LES AND RANS COMPUTATIONS FOR THE STUDY OF CONTAMINANT DISPERSION IN THE M.U.S.T FIELD EXPERIMENT

Anne Dejoan[1][*], Jose Luis Santiago[2], Alfredo Pinelli[1], Alberto Martilli[2]
[1]Energy Department, CIEMAT, Madrid, Spain
[2]Environment Department, CIEMAT, Madrid, Spain

1 INTRODUCTION

Air quality is a growing concern in urban environment and accurate prediction of transport and dispersion of contaminants is needed. However, the complex surface topography (buildings and other obstacles) that forms the urban canopy makes difficult the study of such physical process. The interaction between the atmospheric turbulent boundary layer and the urban geometry generates complex flow patterns that determine the distribution of urban pollutant concentration. Measurements of the dispersion of pollutant in urban areas or around obstacles have been carried on in wind or water tunnel experiments by Meroney *et al.* (1996), Yee *et al.* (2006), Castro *et al.* (2006), Bezpalcová & Harms (2005) as well as in field experiments by Biltoft (2001). The traditional models based on Gaussian plume methods, widely used in application for simple terrain, perform poorly for the prediction of urban environment dispersion because the complex geometry formed by bluff bodies such as buildings has to be explicitly described to correctly represent the interaction between the urban canopy and the atmospheric flow. The computational fluid dynamics (CFD) approach is more appropriate for the simulation of urban dispersion phenomena. An "exact" numerical approach would rely upon the use of direct numerical simulation (DNS), where all the scales of the turbulence motion are resolved, thus allowing for the obtention of very detailed informations on the flow field. However, due to its computational cost, DNS is still restricted to the study of turbulent flow around isolated buildings or around a limited number of obstacles (Yakhot *et al.* (2006), Coceal *et al.* (2006)). On the other hand, the Reynolds-average Navier-Stokes (RANS) approach integrates the whole turbulence spectrum so that turbulence modeling assumptions are required for the statistical closures. This approach does not require large CPU resources and has been used by Santiago *et al.* (2007) and by Milliez & Carissimo (2007), for the calculation of

---
* *Corresponding author address*: Anne Dejoan, CIEMAT, Dept. Energía, Ed. 20, Avenida Complutense 22, 28040 Madrid, Spain, *e-mail*: anne.dejoan@ciemat.es

flow over idealized urban geometries. An intermediate approach is the large eddy simulation (LES) methodology which, by means of a filtering operation applied to the Navier-Stokes equations, resolves explicitly the dynamics of the unsteady large scales of turbulence while modeling the small scale motions. Application of LES in urban environment has been pursued by Cheng *et al.* (2003), and Xie & Castro (2007) in flows over an array of regular cubes and by Camelli *et al.* (2005) and by Tseng *et al.* (2006) in field scale flows. Tseng *et al.* (2006) reported that the minimum resolution required to make applicable the use of LES in atmospheric boundary layer flow over urban canopy requires a number of 6-8 grid points across the buildings.

In the present study both RANS and LES approaches are used to simulate the Mock Urban Setting Test (MUST) field experiment. The MUST experiment was set up in the great basin desert (USA) to investigate the dispersion of a passive scalar within a model of a urban environment represented by an almost regular array of rectangular containers (Biltoft, 2001). The purpose of the present study is to assess the applicability of LES in urban canopy flows and to compare it with RANS. In order to make use of a reasonable computational time, the LES presented herein have been performed in the limit of the grid resolution suggested by Tseng *et al.* (2006). The assessment is done through a comparative analysis of the results on the mean velocity field and mean concentration obtained with LES and RANS against the experiments data. The analysis includes effects of geometrical irregularities on the flow and of small deviation of the inflow wind-direction on the pollutant plume dispersion.

2 COMPUTATIONAL PROCEDURE

2.1 Flow equations and numerical method

In both LES and RANS calculations a neutral turbulent flow was considered without including buoyancy and stratification effects.

In the LES approach, the large-scale flow motions are

described by the filtered incompressible Navier-Stokes equations

$$\frac{\partial \overline{U}_i}{\partial t} + \frac{\partial \overline{U}_j \overline{U}_i}{\partial x_j} = -\frac{\partial \overline{P}}{\partial x_i} + \nu \frac{\partial^2 \overline{U}_i}{\partial x_j \partial x_j} - \frac{\partial \tau_{ij}}{\partial x_j} \quad (1)$$

where $\overline{U}_i$, $\overline{P}$ define the filtered velocity component and the filtered pressure, respectively, and ν is the fluid kinematic viscosity. The contribution of the subgrid-scale represented by the stress tensor τ_{ij} is modeled by the standard Smagorinsky model

$$\tau_{ij} = -2\nu_{sgs}\overline{S}_{ij} = (C_s\Delta)^2|\overline{S}|\,\overline{S}_{ij} \quad (2)$$

where $\overline{S}_{ij} = 0.5(\partial U_i/\partial x_j + \partial U_j/\partial x_i)$ is the filtered strain tensor and ν_{sgs} the subgrid-scale viscosity. The Smagorinsky constant C_s is set to the value 0.1 and the filter width, Δ, is deduced from the grid computational size. Regarding the concentration, its evolution is given by the filtered passive scalar equation

$$\frac{\partial \overline{C}}{\partial t} + \frac{\partial \overline{U}_j \overline{C}}{\partial x_j} = D\frac{\partial^2 \overline{C}}{\partial x_j \partial x_j} - \frac{\partial \sigma_j}{\partial x_j} \quad (3)$$

where $\overline{C}$ is the filtered concentration and D is the scalar diffusivity. The subgrid-scale scalar stress σ_j is modeled via an eddy viscosity formulation as well,

$$\sigma_j = -\frac{\nu_{sgs}}{Sc_{sgs}}\frac{\partial \overline{C}}{\partial x_j} \quad (4)$$

where Sc_{sgs} defines the turbulent subgrid-scale Schmidt number. Following the work by Neto *et al.* (1993), the Sc_{sgs} value has been set to 0.6. This value implicitly implies that the characteristic length scale of the subgrid-scale turbulent fluctuations of the passive scalar is of the same order of the subgrid-scale turbulent flow motions.

The LES simulations were performed using as baseline code the open source CFD code based on the Field Operation and Manipulation C^{++} class library for continuum mechanics (OpenFOAM, 2006). The numerical method used for integrating Eqs. 1-3 is based on the finite volume method formulated in a collocated grid arrangement. A Pressure Implicit Splitting of Operators (PISO) algorithm with two corrector steps is used to couple the velocity and the pressure (which ensures mass conservation). An incomplete-Cholesky preconditioned biconjugate gradient algorithm is used to solve the linearized equations of the velocity components while an algebraic multi-grid solver is used for the discretized pressure Poisson equation. A Rhie-Chow interpolation is used for the pressure gradient terms to avoid pressure oscillations due to the collocated grid arrangement. The temporal integration is performed by using the second-order semi-implicit backward scheme and the spatial derivatives are discretized according to the second-order central differencing scheme. In the case

of the concentration, the bounded total variation scheme was used for the convective terms in order to maintain positive the concentration values.
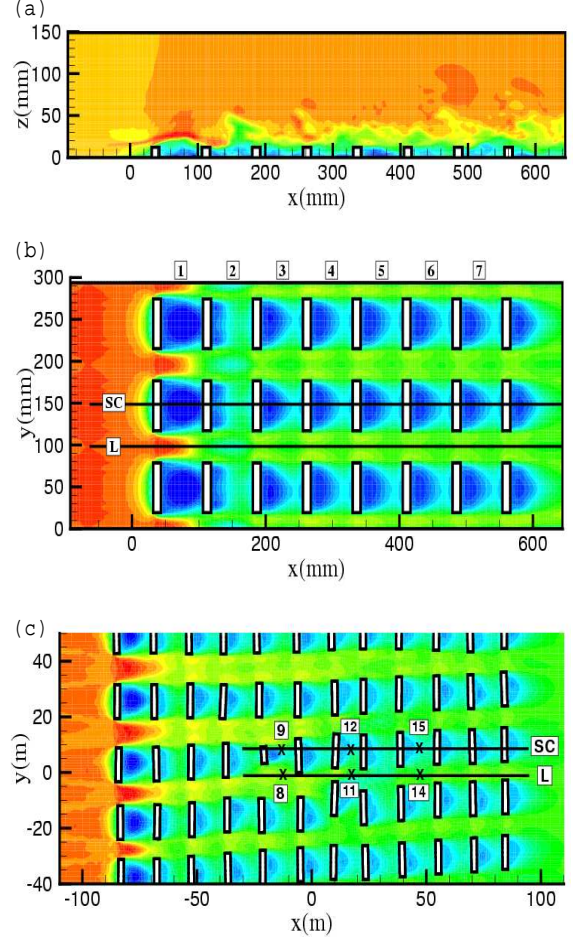
Figure 1: Flow geometries, LES: (a) isocontours of the instantaneous streamwise velocity in the plane (xOz) at y=150 mm and (b) of the mean streamwise velocity in the plane (xOy) at z= 6mm, in the regular MUST geometry; (c) detailed view of the isocontours of the mean streamwise velocity in the plane (xOy) at the z=1.2m in the irregular MUST field geometry. For each plot 20 isocontours between the minimum and maximum velocity are drawn.

The RANS calculations were carried on by making use of FLUENT code to solve the steady incompressible Reynolds-averaged Navier-Stokes equations. The evolution of the mean concentration is given by a transport equation for a passive scalar contaminant very similar to Eq. 3 in which the filtered flow quantities have to be replaced by the mean flow quantities. The value of

(a)

(b)
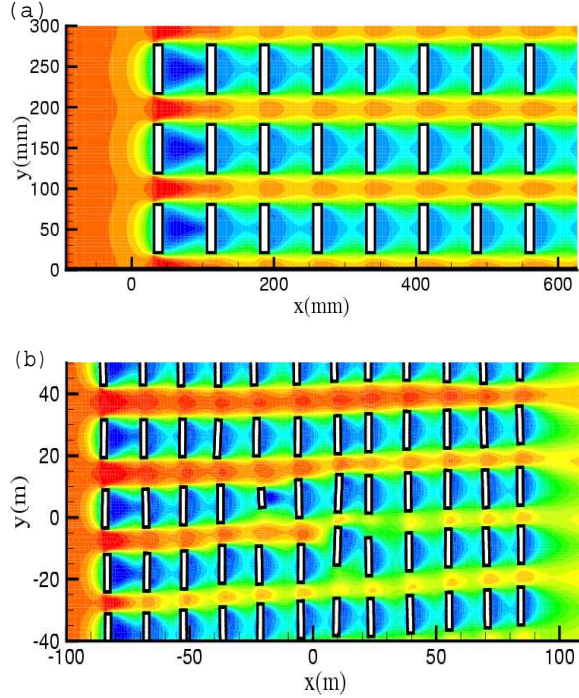
Figure 2: Flow geometries, RANS: (a) isocontours of the mean streamwise velocity in the plane (xOy) at z= 6mm in the regular MUST geometry; (c) zoom of the isocontours of the mean streamwise velocity in the plane (xOy) at the $z=1.2$m in the irregular MUST field geometry. For each plot 20 isocontours between the minimum and maximum velocity is drawn.

the turbulent Schmidt number for the RANS simulations was $Sc_t = 0.9$. The governing equations are solved in a collocated grid system using a finite volume method. The pressure-velocity coupling is solved by means of the semi-implicit method for pressure-linked equations algorithm (SIMPLE) (Patankar, 1980). A second-order up-wind scheme is used for the discretization of the advection terms. The turbulence closure used is the standard $k - \varepsilon$ model. A full description of the equations and numerical method used in the RANS calculations can be found in Santiago *et al.* (2007).

2.2   Flow and computational set up

Two geometries were considered. Firstly, we focussed on a simplified geometry restricted to a limited number of regular containers matrix. Secondly, the geometry of the MUST wind tunnel experiment of Bezpalcová & Harms (2005), which represents a scaled model of the MUST field configuration that includes the irregularities present

in the field campaign measurements, has been considered. For both geometries, computations with a wind direction
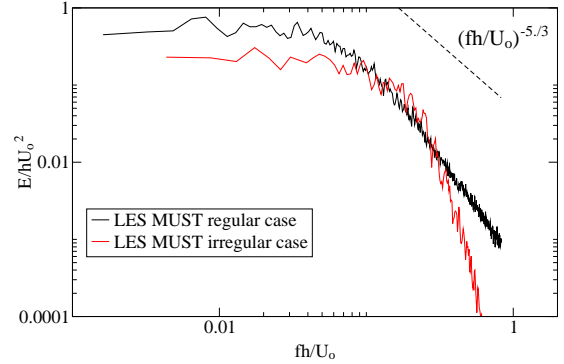
Figure 3: Frequency spectra energy given for the the regular and irregular MUST geometries at the respective locations **SC5** and **SC12** (see Fig. 1)

parallel to the (Ox) axis were performed. These two flow configurations will be termed from now on as "the regular array case" and "the irregular array case", respectively. An overview of these geometries is given in Figs. 1.

Finally, for the calculations of the contaminant dispersion in the near-full scale MUST flow field, the trial 2682353 was selected from the measurements series of Biltoft (2001). In this flow configuration the geometry is identical to the irregular array case except that the wind direction is not aligned with the (Ox) axis but has a deviation of 48±2 degrees with this axis, i.e. 198±2 degrees in the meteorological convention. The release of the passive contaminant is continuous and emitted from the roof of the container located at ($x = -53.43$ m, $y = 48.77$ m). This case will be referred to the "outdoor MUST case". The full geometry of the outdoor case is illustrated on Fig. 10.

In the LES the domain size of the regular case geometry extends over 3 rows of 8 containers. The domain size is $L_x \times L_y \times L_z = 645 \times 294 \times 149$ mm³ and a number of points $N_x \times N_y \times N_z = 232 \times 78 \times 75$ is used for the computational grid in the streamwise, spanwise and vertical directions, respectively. Each container has a rectangular shape of 74.7 mm long, 14.8 mm wide and 12.4 mm height, and is discretized using $16 \times 5 \times 12$ points. A regular mesh is used in the (Ox) and (Oy) directions while a stretched one with an aspect ratio not exceeding 1.1 is used in the vertical direction. The full field geometry
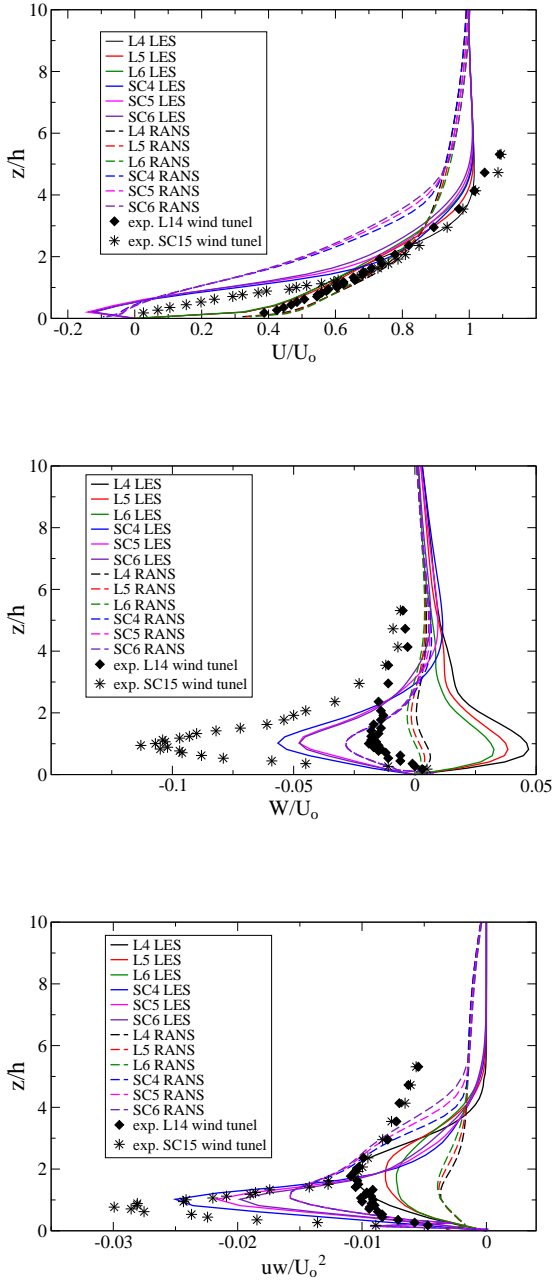
Figure 4: Regular array geometry: comparisons between LES, RANS and experiments of the normalized streamwise and vertical velocity components, U/U_o and W/U_o, and of the Reynolds shear-stress, uw/U_o, given at different locations along the line **L** and **SC**, see Fig. 1.

(used in the irregular array and outdoor MUST cases) covers a domain of dimension $L_x \times L_y \times L_z = 315 \times 300 \times 21$ m^3 discretized with 1.6×10^6 points. Each container is 12.2 m long, 2.42 m wide and 2.54 m height and, on the average, described by $11 \times 4 \times 10$ points.

In the RANS calculations the domain size of the regular-array geometry is $L_x \times L_y \times L_z = 1143.5 \times 489.5 \times 136.4$ mm^3. This domain covers 5 rows of containers (i.e an array of 12 x 5 containers). The number of grid cells used is $N_x \times N_y \times N_z = 255 \times 125 \times 40$. Each container is discretized by 15 cells in streamwise direction, 5 cells in the spanwise direction and 10 cells in the vertical direction. The grid employed to discretize the computational domain of the field geometry in the RANS calculations is similar to the LES one.
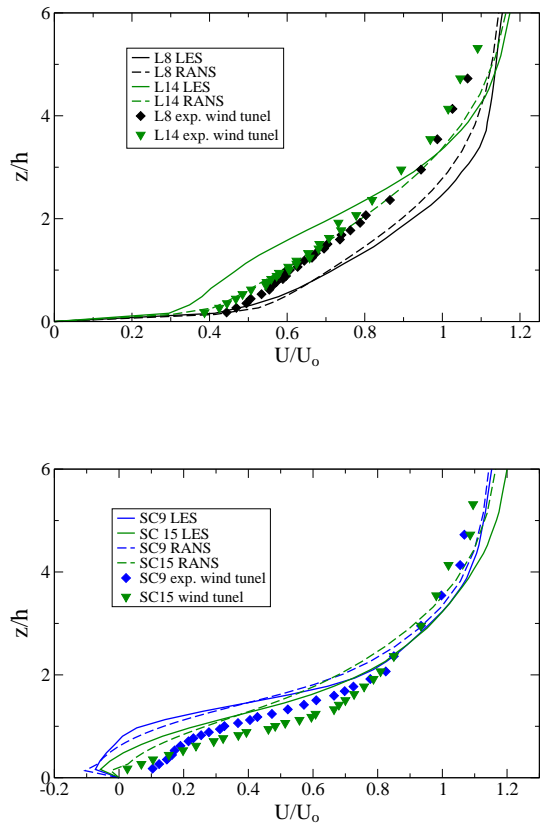
Figure 5: Irregular array geometry: comparisons between LES, RANS and experiments of the normalized streamwise velocity component, U/U_o, given at different locations along the lines **L** and **SC** (see Fig. 1)
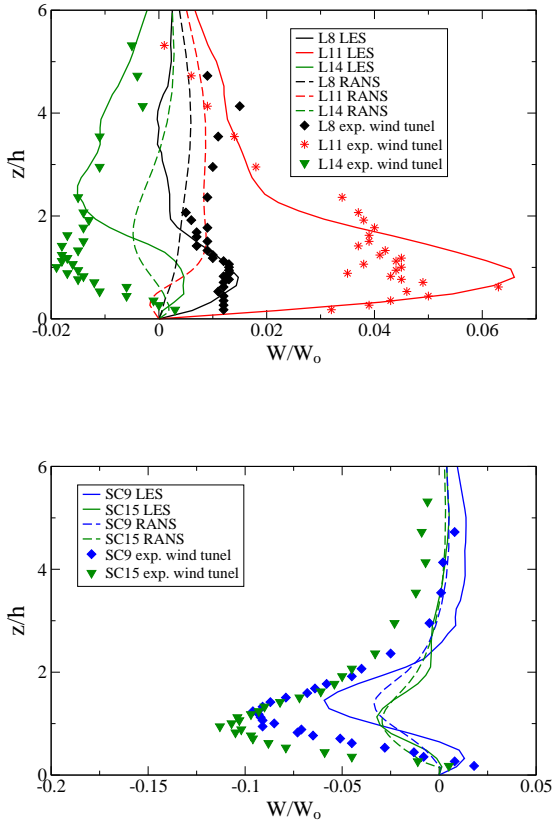
Figure 6: Irregular array geometry: comparisons between LES, RANS and experiments of the normalized mean vertical velocity component, W/U_o, given at different locations along the lines **L** and **SC** (see Fig. 1)

Figure 7: Irregular array geometry: comparisons between LES, RANS and experiments of the normalized mean Reynolds shear stress, uw/U_o^2, given at different locations along the lines **L** and **SC** (see Fig. 1)

At both the bottom boundary ($z = 0$) and the surface container, a zero vertical velocity and a logarithmic type boundary condition for the tangential stresses is used. The terrain surface roughness was modeled in the RANS approach but not in the LES. However, it has been observed that the effect of roughness inside the array of obstacles has a very little influence on the RANS velocity field. At the top of the domain a free-slip boundary condition is applied. At the lateral boundary conditions of the regular geometry, a symmetry type boundary condition is imposed. In the LES, the inflow consists of a mean velocity to which random fluctuations are added to simulate unsteadiness inflow turbulence. The inlet boundary is located upstream of the first line of obstacles, at a distance of $10h$ and $25h$ (with h defining the height container) for the respective regular array case and irregular/field array. The inflow condition in the RANS calculations is fitted from the experimental data and located at $8h$ and $25h$ upstream of the first line of containers in the regular

and irregular array geometries, respectively. For both LES and RANS computations, the outflow boundary condition consists of a fixed pressure with a no-gradient condition for the velocity. In the regular array geometry the outflow condition is imposed at $6h$ downstream of the last line of containers in the LES and at $15h$ in the RANS. In the irregular array geometry, the outflow is located at $30h$ downstream of the final obstacles line. The release of contaminant was done by adding in the transport equation of the contaminant a locale source term that imposed a flux with a value identical to the experiments, $Q = 225$ l/m. As far as the concentration is concerned, a no-gradient boundary condition was used at the surface containers and at the bottom, top and exit of the computational domain.

The Reynolds number, based on the inlet velocity, U_o, the height of the container, h, and the kinematic viscosity, ν, is $R_e = U_o h/\nu = 4700$ in the regular array case and $R_e = 10^6$ in the irregular array and outdoor cases. The

time step used in the LES is such that the Courant number do not exceed 0.6. The energy spectra given on Fig. 3 for the irregular and regular geometry cases at two locations behind the containers indicate that, for each flow simulation, the largest frequencies of the resolved turbulence scales are well located in the inertial range. Compared to the irregular array flow case, the spectra of the regular array flow case exhibits a larger inertial range as a consequence of the lower Reynolds number and higher grid resolution used in this simulation.

The LES runs were performed using 8 nodes on a multi-processors SGI Altix 3700 computer. The CPU time value is between 15-18 s/iteration/processor for both the regular and irregular geometries. The mean statistics extracted from the LES were accumulated over several "through flow" time units, $T = L_x/U_o$, after having reached a satisfactory developed turbulent field. For the regular geometry case the statistics were performed over a total time of $40T$, while in the case of the irregular and outdoor geometry cases a total statistical time of 15 was used. This corresponds to an average of three weeks computations to extract the statistical field flow quantities. The RANS calculations run on a mono-processor on a SGI origin 3800 and required in average one day CPU.
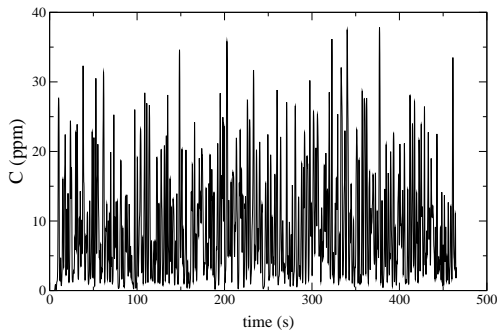
Figure 8: Outdoor MUST real field flow configuration, wind-direction angle=198°: time evolution of the instantaneous concentration at the location ($x = -45.5$m, $y = 14.84$m, $z = 1.6$m)

3 RESULTS

The presentation of the results is twofold. First, a comparison between LES, RANS and experimental data is given for the velocity and turbulence fields in the case of a flow approaching the array of obstacles with a direction parallel to the (Ox) axis (referred as wind direction at angle $\alpha = 0$). This comparison aims to get some insight on the effects of introducing geometrical irregularities and
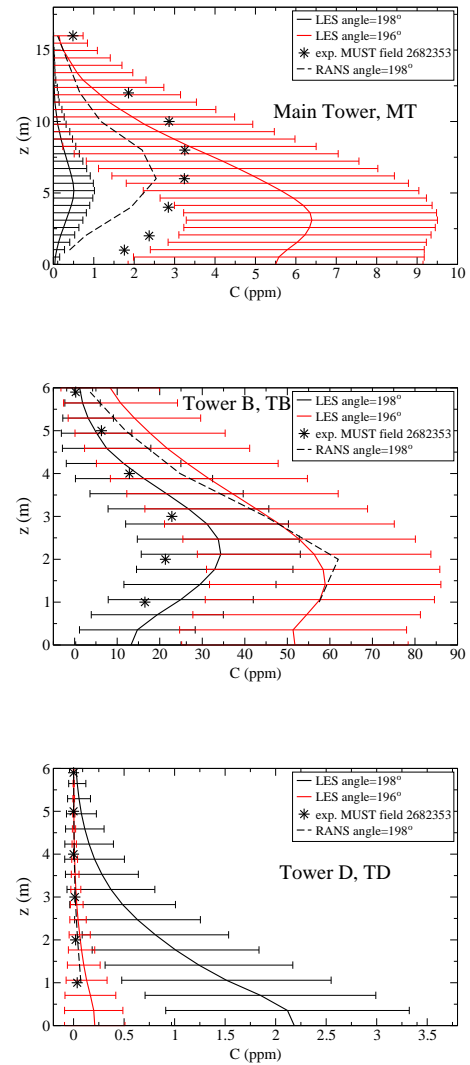
Figure 9: Outdoor MUST field flow configuration: concentration profiles given for the two wind-direction angles: $198°$ and $196°$. The bars represent the standard deviation of the concentration

how far their inclusion is relevant for the computation of such flows. Second, the results on the contaminant dispersion obtained from the LES and RANS for the outdoor MUST case with a non-aligned wind direction with the (Ox) axis is presented. In this analysis the effects of small variation of the inflow wind-direction on the plume dispersion is addressed.

The mean velocity and turbulence field quantities are normalized by the streamwise velocity value, U_o, taken at the locations considered at the height $z \sim 110$ mm ($\sim 9h$) in the regular array case. Regarding the irregular

array, the reference velocity to normalize the data is the streamwise inlet velocity taken at the height $z \sim 7.29$m ($\sim 3h$). The height of the obstacle h was chosen as the normalization length scale.

3.1 Regular array case, angle $\alpha = 0$

The profiles of the mean streamwise and vertical velocity components, U/U_o and W/W_o, and of the Reynolds shear stress, uw/U_o^2, are compared in Figs. 4 at different locations along the line **L** and **SC** (see Fig. 1). The comparisons show that RANS and LES exhibit only slight variations of the mean velocity and of the Reynolds shear stress profiles along the two position lines. Downstream of the locations **L4** and **SC4** the mean and turbulence flow quantities are very similar regardless the locations considered. This is also indicated by the repeated flow patterns observed in the LES and RANS from the isocontours of the mean streamwise velocity component drawn for the regular array case on Figs. 1 and 2. This suggests that the inflow condition is only influential in the first lines of obstacles but that, further downstream, does not affect the flow. Therefore, the comparisons at the locations **L5**-**L6** and **SC5**-**SC6** can be done without considering inflow condition effects. This behavior was previously reported by Meinders & Hanjalić (1999) in the experiments of a flow over a regular array of cubes.

When comparing LES and RANS it is observed that the recirculation zone behind the containers (deduced from the negative near-wall values of U/U_o at the locations **SC5** and **SC6**) is larger in LES than in the RANS calculations as well as the negative peak of W/W_o and of the Reynolds shear stress, uw/U_o^2. In general, the RANS approach tends to strongly underpredict W/W_o and uw/U_o at the locations **L5** or **L6**.

To get some insight on how far the computational results of a flow over a regular array can be compared with experimental data that includes geometrical irregularities, Figs. 4 includes as well the experimental data extracted from the wind tunnel campaign measurements at the locations **L14** and **SC15** (see Fig. 1c). These two locations are the only one available but nevertheless, they are well positioned inside the obstacles array and far downstream of the small container located close to **SC9**. The experimental data for the profiles of U/U_o and of uw/U_o^2 compare quite well with the calculations, a better agreement being observed with LES. However, large discrepancies are observed between the experiments and the LES/RANS computations for the profiles of W/W_o, in particular along the line **L**. It will be shown in the next section that this discrepancy is a consequence of the geometrical irregularities.

3.2 Irregular array case, angle $\alpha = 0$

Figs. 5-6-7 show the comparisons of the mean velocity and Reynolds shear stress profiles between LES, RANS and experimental data obtained for the irregular array case. The experimental data exhibit a high dependence of the geometrical irregularities upon the W/W_o velocity component along the line **L** but not upon the flow quantities U/U_o and uw/U_o^2 which show moderate variations along this line.
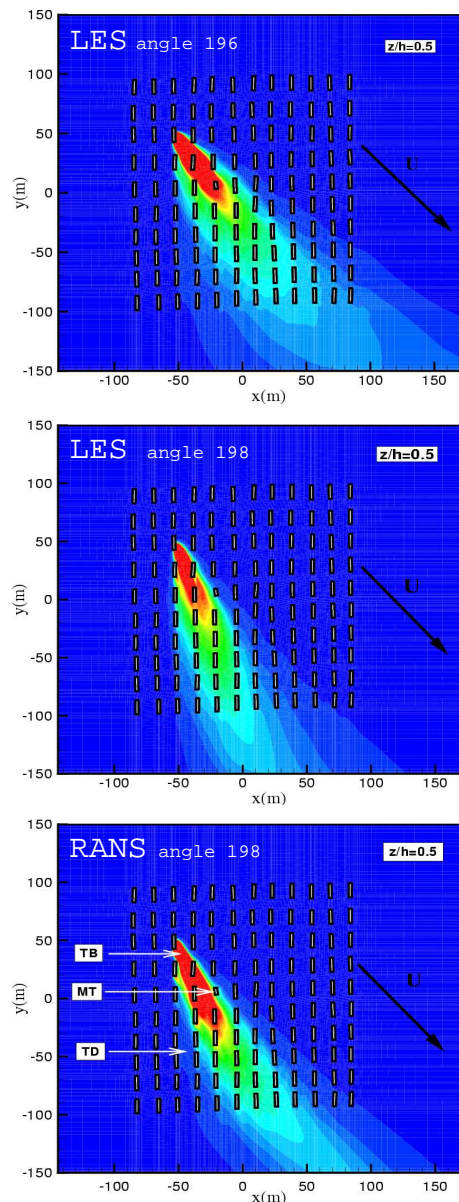
Figure 10: Outdoor MUST field flow configuration: comparison between LES and RANS of the mean plume spatial propagation at the plane z/h=0.5. For each plot 20 isocontours are drawn in the range [0;8ppm]

Along the line **SC** the irregularities effects are quite low, at least at the locations considered here. The computed U/U_o and uw/U_o profiles show higher variations along the line **L** than the experiments while along the **SC** the variations are lower. The U/U_o profiles predicted by LES tend to be closer to the RANS results than to the experiments, except at the location **L14** where the RANS approach gives a profile very close to the experiments. The closer similarity between LES and RANS observed here as opposed to the regular array case, is probably due the coarser grid resolution used in the present flow configuration. However, regarding the velocity W/W_o the predictions given by the LES are in better agreement with the experiments than the RANS, in particular along the line **L** and at the location **SC9**. Both LES and RANS uw/U_o^2 profiles fit the experimental data at the locations along the line **SC**.

3.3 Outdoor MUST case, angle $\alpha = 196°, 198°$

The measurements of the trial 2682353 selected for the present calculations reported a variation of the mean wind-direction angle between $196°$ to $200°$ when moving from the height of $z = 4$ m to $z = 16$ m. Previous LES of pollutant dispersion in the outdoor MUST configuration have shown that concentrations levels were sensitive to small angle deviation of the inflow wind-direction angle (see Camelli *et al.* (2005)). To take into account these effects, two cases have been carried out in the present LES: one case with an inflow wind-direction angle α set up to $196°$ and another case with an angle $\alpha = 198°$. The RANS calculation of the outdoor MUST configuration has been performed with the wind-direction angle $\alpha = 198°$. The unsteady character of the LES approach reveals strong fluctuations of the concentration as shown by its time evolution given in Fig. 8 where events with high deviation from the mean value are observed. The RANS approach cannot provide such information. Figure 8 also indicates the necessity to include the standard deviation of the contaminant concentration in the analysis of the results.

Figure 9 compares the mean concentration profiles obtained from LES and RANS with the measurements at the three locations that are displayed on the plot at the bottom of Fig. 10. For each LES the standard deviation of the concentration is included. The shape of the computed concentration profiles agrees well with the experiments. For the wind-direction angle $\alpha = 198$ °, LES gives a better agreement with the measurement at the tower TB, while at the tower MT and TD, the RANS provides quite good results. This behavior is explained by the higher deviation of the plume contaminant given by the RANS computations when compared with the LES (see Fig. 10). Nevertheless, by comparing the profiles obtained for the two angles $\alpha = 196°$ and $\alpha = 196°$, the concentration

levels given by the present LES shows a high influence of small deviation angle of the inflow wind-direction as reported by Camelli *et al.* (2005). The slight deviation of the wind-direction angle tends to give a better agreement between the LES and the experiments at the towers MT and TD. The relative high deviation of the plume dispersion between $\alpha = 196°$ and $\alpha = 198°$ is clearly shown on the top and middle isocontours plots given on Fig. 10. At the tower TB, the RANS overpredicts the mean concentration when compared to the measurements but is close to the LES performed with $\alpha = 196°$. To complete this analysis a RANS calculation with an inflow wind-direction $\alpha = 196°$ would be necessary.

4 CONCLUSION

The present comparative study showed that the inclusion of geometrical irregularities is influential for the prediction of the vertical velocity but that these effects are still moderate for the streamwise velocity and the Reynolds shear stress at least at the locations considered. In both regular and irregular array flow configurations, the RANS approach shows a general tendency in underestimating the vertical velocity and Reynolds shear stress, in particular at locations between two lines of containers. This deficiency is improved by using the LES approach. Regarding the streamwise velocity, the RANS and LES give similar results, when using a similar grid.

The computational study on the dispersion of pollutant in the near-full field scale MUST leads to the conclusion that, at least in the LES approach, the effects of small deviation of the inflow wind-direction can induce large variations of the concentration. When including the angle deviation effects and the standard deviation of the concentration, LES provides results that cover the measurements and the RANS data. In this flow configuration the RANS approach performs quite well and give predictions that are in a correct agreement with the experiments. This analysis suggests to further explore the sensitivity of the RANS approach to small angle deviation of the wind-direction inflow. As a general conclusion it is possible to state that the RANS approach provides correct predictions on mean flow quatities and is still an appropriate methodology in this respect considering the low CPU cost. However, in some applications like those involving dispersion of toxic agent, estimates of mean concentrations are not sufficient. In such cases it is also of importance to predict the probability of events that present levels of pollutant with high departure from the mean values. Such relevant information can not be provided by RANS but can reasonably be predicted by LES.

REFERENCES

Bezpalcová, K., Harms. F., 2005: EWTL Data Report / Part I: Summurized Test Description Mock Urban Setting Test. Environmental Wind Tunnel Laboratory, Center for Marine and Atmospheric Research, University of Hamburg.

Biltoft, C. A., 2001: Customer report for Mock Urban Setting Test (MUST). DPG Document WDTC-TP-01-028, West Desert Test Center, U.S. Army Dugway Proving Ground, Dugway, Utah, pp.58

Camelli, F.E., Lohner, R., Hanna, S.R., 2005: VLES Study of MUST experiment. 43rd AIAA Aerospace Meeting and Exhibit, January 10-13, Reno, Nevada, paper 1279

Castro, I. P., Cheng, H., Reynolds, R., 2006: Turbulence over urban-like roughness: deductions from wind-tunnel measurements. Boundary Layer Meteorol., **118**, pp. 109-131

Cheng, Y., Lien, F.S., Yee, E., Sinclair, R., 2003: A comparison of large eddy simulations with a standard k-ε Reynolds-averaged Navier-Stokes model for the prediction of a fully developed turbulent flow over a matrix of cubes. J. Wind Eng. Indust. Aero., **91**, pp. 1301-1328

Coceal, O., Thomas, T. G., Castro, I. P., Belcher, S. E., 2006: Mean flow and turbulence statistics over groups urban-like cubical obstacles. Boundary-Layer Meteorol., **10.1007/s10546-006-9076-2**, on line

Fluent Inc (2005), FLUENT 6.2 User's guide, volumes 1-3, Fluent Inc, Lebanon, pp. 2216

Meinders, E. R., Hanjalić, K., 1999: Vortex structure and heat transfer in turbulent flow over a wall-mounted matrix of cubes. Int. J. of Heat and Fluid Flow, **20**, pp. 255-267

Meroney, R.N., Pavegeau, M., Rafailidis, S., Shatzmann, M., 1996, Study of line source characteristics for 2-D physical modelling of pollutant dispersion in street canyons. J. Wind Eng. Indust. Aero., **62**, pp. 37-56

Milliez, M., Carissimo, B., 2007: Numerical simulations of pollutant dispersion in an idealized urban area, for different meteorological conditions. Boundary-Layer Meteorol. **122**,2, pp. 321-342

Neto, A. S., Grand, D., Métais, O., Lesieur, M., 1993: A numerical investigation of the coherent vortices in turbulence behind a backward-facing step. J. Fluid Mech., **256**, pp. 1-25

OpenFOAM (2006) Version 1.3, User and Programmer guide. Technical Report, http://www.opencfd.co.uk/openfoam

Santiago, J.L, Martilli, A., Martin, F., 2007: CFD simulation of airflow over a regular array of cubes. Part I: Three-dimensional simulation of the flow and validation with wind-tunnel measurements. Boundary-Layer Meteorol., **122**,3, pp. 609-634

Tseng, Y-H., Meneveau C., Parlange M., 2006: Modeling flow around bluff bodies and predicting urban dispersion using large eddy simulation. Environ. Sci. Technol., **40**, pp. 2653-2662

Xie, Z., Castro, I. P., 2007: LES and RANS for turbulent flow over arrays of wall-mounted obstacles. Boundary Layer Meteorol., in press

Yakhot, A., Anot, T., Liu, H., Nikitin, N., 2006: Direct numerical simulation of turbulent flow around a wall-mounted cube: spatio-temporal evolution of large-scale vortices. J. Fluid Mech. **566**, pp1-9.

Yee, E., Gailis, R.M., Hill, A., Hilderman, T., Kiel, D., 2006: Comparison of wind tunnel and water-channel simulations of plume dispersion though a large array of obstacles with a scaled field experiment. Boundary-Layer Meteorol., **121**, pp. 389-432